Topological Data Analysis for Electric Motor Eccentricity Fault Detection

Wang, Bingnan; Lin, Chungwei; Inoue, Hiroshi; Kanemaru, Makoto

TR2022-130 October 19, 2022

Abstract

In this paper, we develop topological data analysis (TDA) method for motor current signature analysis (MCSA), and apply it to induction motor eccentricity fault detection. We introduce TDA and present the procedure of extracting topological features from time-domain data that will be represented using persistence diagrams and vectorized Betti sequences. The procedure is applied to induction machine phase current signal analysis, and shown to be highly effective in differentiating signals from different eccentricity levels. With TDA, we are able to use a simple regression model that can predict the fault levels with reasonable accuracy, even for the data of eccentricity levels that are not seen in the training data. The proposed method is model-free, and only requires a small segment of time-domain data to make prediction. These advantages make it attractive for a wide range of fault detection applications.

Annual Conference of the IEEE Industrial Electronics Society (IECON) 2022

Topological Data Analysis for Electric Motor Eccentricity Fault Detection

Bingnan Wang and Chungwei Lin
Mitsubishi Electric Research Laboratories (MERL),
201 Broadway, Cambridge, MA 02139 USA
Email: bwang@merl.com

Hiroshi Inoue and Makoto Kanemaru
Advanced Technology R&D Center,
Mitsubishi Electric Corporation,
Amagasaki, Japan

Abstract—**In this paper, we develop topological data analysis (TDA) method for motor current signature analysis (MCSA), and apply it to induction motor eccentricity fault detection. We introduce TDA and present the procedure of extracting topological features from time-domain data that will be represented using persistence diagrams and vectorized Betti sequences. The procedure is applied to induction machine phase current signal analysis, and shown to be highly effective in differentiating signals from different eccentricity levels. With TDA, we are able to use a simple regression model that can predict the fault levels with reasonable accuracy, even for the data of eccentricity levels that are not seen in the training data. The proposed method is model-free, and only requires a small segment of time-domain data to make prediction. These advantages make it attractive for a wide range of fault detection applications.**

Index Terms—**Electric Machines; Fault Detection; Machine Learning; Topological Data Analysis**

I. Introduction

Electric motors are widely used in many aspects of the modern society, such as factories, household appliances, electric vehicles, etc. The condition monitoring and fault detection of these machines are becoming more important with the growth of internet of things. Among many different faults that can happen in a motor, eccentricity is one common type of fault that corresponds to the non-uniform gap between the stator bore and the rotor. Eccentricity faults can be categorized into three types: the static eccentricity, the dynamic eccentricity, and the mixed eccentricity. Static eccentricity occurs when the center of the rotor is deviated from the central axis of the stator bore, while the rotation center is still aligned with the center of the rotor. Dynamic eccentricity occurs when the rotation center and the stator bore central axis still align, but the rotor center is displaced. Mixed eccentricity is a combination of both static eccentricity and dynamic eccentricity [1].

There are many reasons that can cause motor eccentricity, and the air gap eccentricity can in turn damage other parts of the motor and cause breakdown of the machine if not corrected in time. During the manufacturing stage, it is not feasible to produce motors with zero air gap eccentricity. Static eccentricity may exist due to the imperfect alignment between stator core assembly and the rotation center, or the deviation of the stator core from a perfect circle. Similarly, a small dynamic eccentricity can also exist due to the imperfect alignment between center of the rotor and the rotation axis, or imperfect shape of the rotor. Through the operating lifetime of a motor, the eccentricity level can increase, for example, due to bearing degradation, or the mechanical degradation of the mount, causing physical shift of the stator assembly. The air gap eccentricity induces unbalanced magnetic pull (UMP), which works against rotor stiffness and may cause stator winding faults and rubbing between rotor and stator with increased eccentricity, eventually leads to machine failure. It is therefore important to check electric motors for eccentricity both in the production stage for quality control, and throughout operation for the safety and asset protection.

Extensive research efforts have been put into the detection of eccentricity faults in the past decades [2]–[6], with vibration analysis and motor current signature analysis (MCSA) being two leading methods. Recently, machine learning and deep learning techniques have been applied to the fault detection and classification of electric machines based on measured vibration signals [7]. However, vibration signals can often be influenced by noises from other sources, such as the mechanical unbalance of the motor, the excitation from external sources in complicated factory setting. In addition, the sensitivity of vibration analysis also varies depending on the specific sensor installation location on the motor casing. It is therefore challenging to identify eccentricity faults based solely on vibration signals.

MCSA has been proposed to address these problems, which has the additional advantages of simple implementation and cost saving, as no dedicated sensors are required. A lot of work has been dedicated to the detailed modeling of fault signatures for each type of eccentricity using MCSA [8]–[11]. One challenge for eccentricity fault detection using MCSA is that, a lot of the spatial harmonics caused by eccentricity can be reflected in vibration signals, but do not appear in the time harmonics and are thus absent in the stator current. In addition, certain stator current fault signatures can depend on specific motor design parameters and are not universal for all motors. For instance, it has been shown that under certain combinations of stator slot and rotor bar numbers, some fault signatures due to static eccentricity are more difficult to detect [9], [11]. For experimental data analysis, unlike vibration signals, the current components due to eccentricity faults are typically a few orders smaller than the dominating fundamental component at supply frequency. Commonly used machine learning techniques on time-domain signals that have been working well for vibration signals cannot effectively distinguish stator current signals of machines under healthy and faulty conditions. Detailed spectrum analysis of measured stator current signals are typically required to extract frequency components due to eccentricity faults.

Topological data analysis (TDA) is an active research area in computational topology; practically it offers a numerical procedure to extract the shape information from a data space, such as connected components and holes [12]. Generally topological features are invariant under small and continuous deformations, coordinate-free, and therefore more robust against noises. These advantages make TDA attractive in dealing with many challenging data analysis tasks. In recent years, largely enabled by the development of persistent homology [12]–[14], TDA has been applied to a broad range of scientific problems, including image analysis [15], time-series data analysis [16], sensor networks [17], chemistry [18], and material science [19], etc.

While mainstream applications of TDA utilize the persistent homology method to reveal major shapes in data spaces, and either ignore smaller features or consider them as noises, we use it in an opposite way, by filtering out the main shape and focusing on the small features of the time-series stator current in the persistent homology. We show that the extracted topological features do contain the fault signatures: there are robust and quantitative differences between data from the same motor with different static eccentricity levels; the mapping between the topological features and the eccentricity levels can thus be used to predict the eccentricity fault.

The rest of the paper is organized as follows. In Section II, we introduce persistence homology, Betti sequence, and the TDA calculation process; in Section III we describe the experiment setup for motor eccentricity study and stator current data acquisition; in Section IV, we apply the TDA process to the measured data from different eccentricity levels; in Section V, we present data-driven approach for eccentricity level prediction using the proposed TDA method, with two application scenarios: one for eccentricity level inspection and quality control during manufacturing stage, one for the eccentricity level prediction during the operating lifetime of an electric motor; in Section VI we conclude the paper.

II. Topological Feature Extraction Method

In this section, we introduce the TDA method with persistent homology and the process of generating persistence diagram and Betti sequence from a data space.

The homology of a data space describes the topological features, such as connected components and holes, and persistent homology is a powerful tool to compute those topological features that persist across different scales. Here we give a high-level description of the procedure to obtain the persistent homology of a data space. More rigorous definitions and detailed descriptions on persistent homology can be found in several references [12]–[14].

First we represent the data space with a point cloud, which is formed by data points sampled from the data space.

Second, we identify the simplicial complex of the point cloud, which is a collection of fundamental topological features, or simplices, such as points, edges, triangles, etc. While there are different algorithms of constructing a simplicial complex, Rips complex is commonly used. It is defined with a threshold value, or filtration radius r, and includes only complices with pair-wise Euclidean distance between points no larger than r.

Third, the homology is determined using linear algebra from the constructed simplicial complex. For example, H_0 homology counts the number of connected components, and H_1 homology counts the number of holes.

Lastly, persistent homology is obtained through a filtration process, by computing the homology with different threshold value r, and tracking the birth and death of the topological features at corresponding r.

There are different ways of representing persistent homology, and persistence diagram is one of the most popular choices. A persistence diagram is a set of points $(b, d)|b, d \in \mathbb{R}^2$ and $d > b$, where each point corresponds to the birth and death of topological feature in a corresponding family of simplicial complexes. In particular, each point (b, d) denoted a topological features being "born" at radius b and "dead" at radius d. There are different algorithms for the filtration of Rips complexes and the computation of persistence diagrams, with implementations available by several software packages. In this work, we use python library Ripser.py for the computation of persistence diagrams [20].

Since we would like to use the topological features as inputs for regression or machine-learning algorithms, it is more convenient to represent the features by vectors of same length. Betti sequence, or Betti curve, which can be derived from a persistence diagram, is an effective way to achieve that [21], [22]. Assume D is a persistence diagram with a finite number of off-diagonal points, with $\alpha = (b_\alpha, d_\alpha)$ a point in the diagram, and maximum filtration radius $r_{max} > 0$, let $\{r_i\}_1^M$ be equally spaced points within $[0, r_{max}]$, the Betti sequence of D is a vector of length M defined as $\vec{\beta} = (\beta_i)_1^M$, with the entries β_i count the number of points in the persistence diagram at filtration radius r_i around the point clouds in the data space. If we define the function:

$$f_\alpha(r) = \begin{cases} 1, & b_\alpha \le r \le d_\alpha \\ 0, & \text{otherwise} \end{cases}$$

Then the points on a Betti sequence is obtained from the summation:

$$\beta_i = \sum_{\alpha \in D} f_\alpha(r_i).$$

III. Experiment Setup & Data Acquisition

In this work, we use a 0.75 kW, three-phase, 2-pole-pair squirrel-cage induction motor for experimental study. The motor has 36 stator slots and 28 rotor bars, and a nominal air gap size of 0.28 mm. The line-to-line voltage and frequency are 200 V and 60 Hz, respectively. As shown in Fig. 1, a few modifications are made to the motor to create different levels

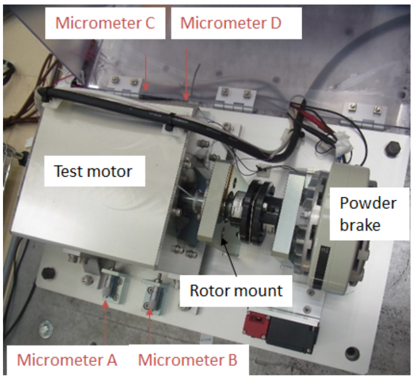

Figure 1. The experiment setup for the study of induction motor eccentricity.

of eccentricity fault. The original bearings of the motor are removed, and the rotor is instead supported by two custom-made mounting structures (only the mount on the load side is visible in the photo) through the extended rotor shaft and a pair of new bearings installed on the mounting structures. The stator assembly of the motor is mounted on a linear stage with its position adjustable in the horizontal direction by two pairs of micrometers. Two pairs of displacement sensors are also installed on the stator facing air gap at the load side and opposite side respectively, to measure the actual air gap size in horizontal and vertical directions when the motor is operating. A power brake is connected to the test motor and serves as load.

With the modified motor setup, different static eccentricity levels in the horizontal direction can be created. In our experiment, a total of 6 eccentricity levels were created when the motor is stand still; data from three phase current sensors and four air gap sensors were recorded for each eccentricity level at 10 kHz sampling frequency under no-load condition. The eccentricity levels were set at 1.5%, 17.2%, 24.1%, 40.5%, 47.1%, 64.6% respectively, with percentage defined as the ratio of the maximum air gap deviation and the nominal air gap size. From the air gap sensor readings, it was shown that the actual static eccentricity of the air gap is very close to the initial settings, with difference within 3% in all cases. In additional, a small dynamic eccentricity level of around 6% exists for all cases according to air gap sensor readings. This mixed eccentricity effect create a side band signal at $f_c = f_s \pm f_r$, where f_s is the supply frequency and f_r is the rotation frequency. From the time-domain current signals, which are shown in Fig. 2, it is difficult to distinguish the eccentricity levels directly as the fundamental component dominates.

IV. TDA on Experiment Data

Now we apply the TDA process established in Section II to the measured stator current signals. The point cloud of the time-domain three-phase current data is naturally formed by sampling the recorded data segment and placing them in 3D Euclidean space. The point clouds of three-phase current data are shown in Fig. 3 for the six eccentricity levels corresponding the time-domain data segments shown in Fig. 2. Since the dominating component of the signals is a periodic wave of fundamental frequency, the most significant shape is a large circle in 3D space. For ideal sinusoidal signals, the formed point cloud shape would be a perfect circle; when other components exist, the points would deviate from the perfect circle. Since the fault components are much smaller in amplitude, it is difficult to tell the different eccentricity levels from the point cloud shapes alone.

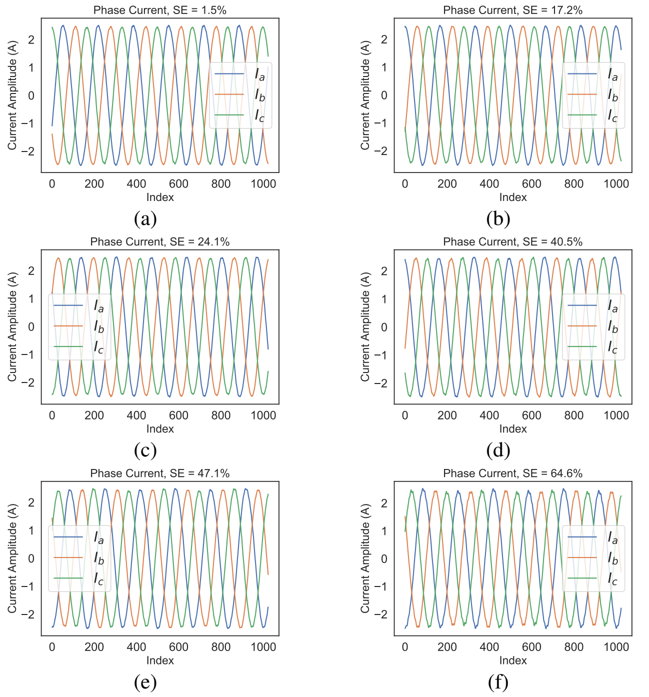

Figure 2. Three phase current signals from six different eccentricity levels. All segments have the same length of 1024 data points.

Fig. 4 shows the computed H_0 and H_1 persistence diagrams of the phase current data for the six different eccentricity levels. The most noticeable differences between these diagrams are the H_1 features, which correspond to the small holes formed by neighboring points. For an ideal sinusoidal wave, there is only one large hole can be formed by its point cloud. When the eccentricity level is small, the deviation from the ideal circle is small, and only a few small features are formed in the H_1 diagram. When the eccentricity level increases, the deviation of the points from the ideal circle is larger, and these points are more likely to form small circles during the filtration process of obtaining the persistence diagram; therefore more and more features show up in the H_1 diagrams with increasing eccentricity level.

While these diagrams are distinct from one another, the number of points in a persistence diagram is not fixed for different input data. So we convert them into Betti sequences of the same lengths: for both H_0 and H_1 sequences, the length is fixed at 1024 whereas the filtration ranges are of [0, 0.07] and [0, 0.14] respectively. Fig. 5 show the computed Betti sequences from the corresponding persistence diagrams. From the H_1 Betti sequences, we can see that the number

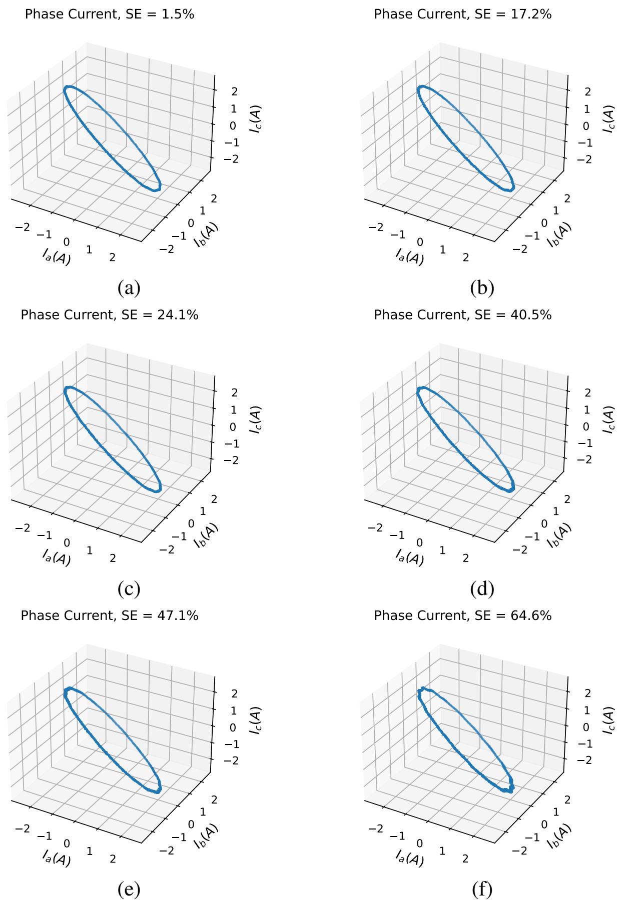

Figure 3. Point clouds of stator current data from six different eccentricity levels corresponding to Fig. 2.

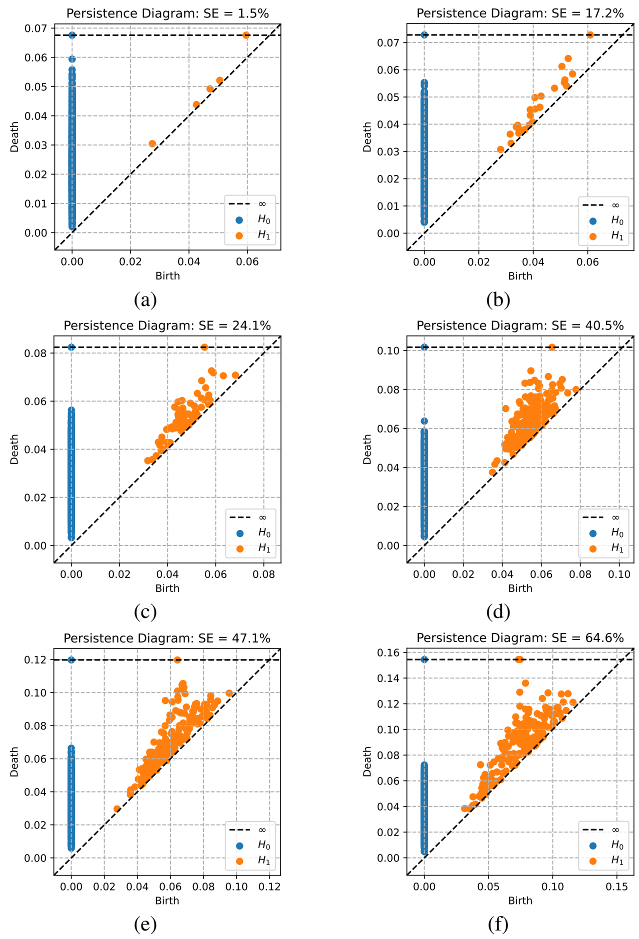

Figure 4. Computed persistence diagrams from phase current data corresponding to the six eccentricity levels.

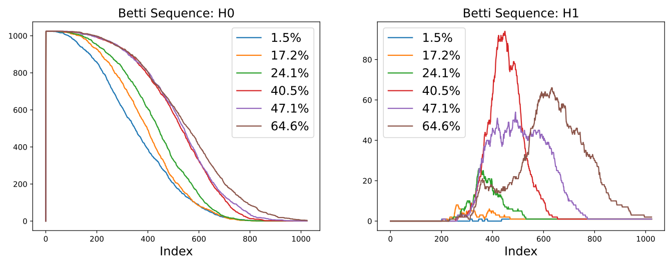

Figure 5. Betti curves corresponding to the H_0 (left) and H_1 (right) persistence diagrams for the six eccentricity levels.

of features as a function of filtration distance changes with eccentricity levels. In addition, while we cannot tell the differences of H_0 features from the persistence diagrams, we can see the trend in the H_0 Betti curves. When the filtration distance is 0, all 1024 data points are not connected, therefore all the Betti curves start at 1024. Upon increasing filtration distance, more and more neighboring points are connected; therefore the number of H_0 features starts to decrease, eventually all points are connected and there is only one feature left. With higher eccentricity level, the amplitude of fault components increases, and the data points are further apart from one another due to their deviation from the large circle (see Fig. 3); therefore the points are connected at a later stage and these H_0 features survive longer, and the area under H_0 Betti curve is monotonically increasing with eccentricity level. We have applied the same analysis to the data generated by circuit simulations and get similar Betti curves, based on which we conclude that the changes in Betti curves are indeed due to eccentricity.

Another important characteristic of persistent homology is its robustness: similar data structure yield similar persistent homology. In Fig. 6, we show that the Betti curves of five different phase current data segments of the same eccentricity level of 64.6%, and they are quite consistent. The similarity of these Betti curves implies that the temporal fluctuations between different samples of time-domain data are filtered out by the proposed procedure, and one could stably extract the fault signature with a relatively short segment of data.

V. TDA for Eccentricity Level Prediction

From above analysis, we can see that TDA is effective in revealing small fault signatures embedded in a large background signal, and separating signals from different fault levels. In this section, we present the use of Betti curves for the data-driven approach of eccentricity fault detection, quantification, and prediction.

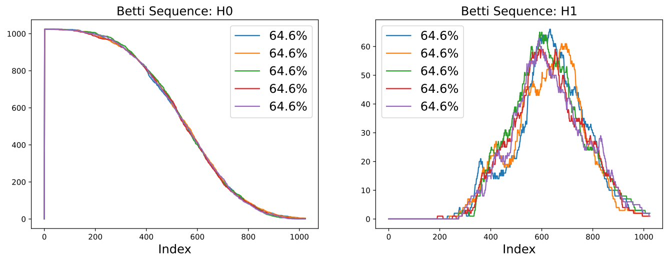

Figure 6. Betti curves corresponding to the H_0 (left) and H_1 (right) persistence diagrams from five different data segments of the same eccentricity level.

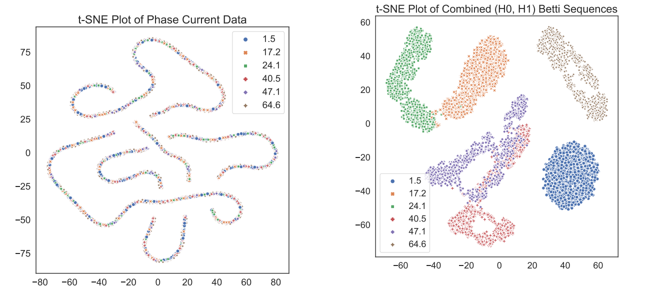

(a) (b)

Figure 7. t-SNE plot in 2d for (a) time-domain phase current data, (b) computed Betti sequences of different eccentricity levels.

The measured data of each eccentricity level is segmented into a total of 1170 samples, each of length 1024 data points, and we apply the established procedure to obtain Betti curves for all these data samples. To visualize the differences of the signals of different eccentricity levels, in Fig. 7 we show the t-distributed stochastic neighbor embedding (t-SNE) plot, which is a commonly used tool to represent the similarities of high-dimensional data in low dimension, of both time-domain phase current data and the computed Betti sequences. With the raw time-domain inputs, data from all eccentricity levels are mixed together, indicating these data segments are similar: they are dominated by the large 60 Hz signal. For both H_0 and H_1 Betti sequences, however, the data samples do cluster according to their respective eccentricity level. We point out that the dominant 60 Hz signal only corresponds to the feature value at very large filtration distance in H_1 Betti sequences, due to the large hole in the point clouds shown in Fig. 3, and has little impact on the profile of the Betti curve. In this sense, the thresholded Betti curve serves as a "nudge filter" that effectively removes the dominant time-domain signal and by doing so it magnifies the behavior of small signals where the fault signatures reside.

We discuss two application scenarios for motor eccentricity fault detection: one in the manufacturing stage, the other through the operation of the motor. In the manufacturing stage, the goal is to inspect the manufactured motors and identify the eccentricity level for quality control purpose. Since many motors of the same model will be mass produced, it makes sense to collect data covering a wide range of eccentricity levels with a test motor, and develop a model to make predictions for new data measured on other motors of the same type. To mimic this scenario, we shuffle the data for all eccentricity levels and split them into training and test sets with a split ratio of 0.8/0.2. Machine learning models are trained on the training dataset, and then applied to the test dataset. While many different models can be developed, we show the results from simple k-nearest neighbor (k-NN) regression model to demonstrate the capability of TDA. For a given new data, k-NN simply search for the nearest neighbors from the training set, and predict the eccentricity level as the average level of these neighbors. As shown in Fig. 8(a), with time-domain phase current data, the model perform poorly on new data, with root-mean-squared-error (RMSE) around 10% and mean-absolute-error (MAE) around 9.4%. On the other hand, as shown in Fig. 8(b), with H_0 Betti sequence, the RMSE is reduced to 1.6% and MAE is reduced to 0.7%. This result shows that the effectiveness of using Betti sequences for interpolation purpose.

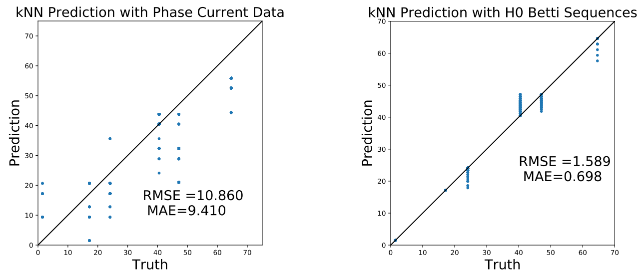

(a) (b)

Figure 8. Prediction of eccentricity level on new data using k-NN model with training data from all six eccentricity levels for (a) phase A current data, and (b) H_0 Betti sequences.

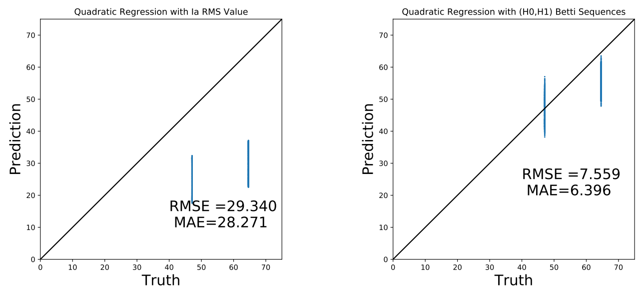

(a) (b)

Figure 9. Prediction of eccentricity level on new data with higher eccentricity levels using regression model with training data from four smaller eccentricity levels for (a) phase A current data, and (b) H_0 Betti sequences.

During the operating lifetime of a motor, we would not have the data for all possible eccentricity levels. Instead, we expect to have measurement data collected during inspections, when eccentricity level is still low. A model can be built based on these earlier measurements, and used to predict the eccentricity level according to later measurements where the fault is expected to become more severe over time. For this task, we assign the experiment data from the four smaller eccentricity levels as training set, and the last two levels as test dataset to check the prediction capability of trained models. Fig. 9(a) and 9(b) show the best prediction result using regression model trained on time-domain current data and Betti sequences respectively. For time-domain data, we extract the RMS value of the phase current and fit a quadratic regression model on training data, and then use it for prediction on new data. The high RMSE and MAE (both close to 30%) indicates the failure of effective prediction. For Betti sequences, we extract the mean values for both H_0 and H_1 sequences, and use them to fit a quadratic regression model, which shows a much improved prediction accuracy, with RMSE and MAE reduced to 8.6% and 7.1% respectively. We have also tested other machine learning models such as supporting vector regression (SVR) models, Gaussian process regression (GPR) models, artificial neural networks (ANNs), and convolutional neural networks (CNNS). However these more involved models tend to overfit on training data and perform worse for extrapolation on new data.

Compared with MCSA, which requires involved domain knowledge and physical model to identify fault signatures, no physical model for the fault is required in the proposed process. We do need labeled data. However, with TDA-processed inputs, data cluster properly according to the fault level, suggesting the possibility of unsupervised learning for fault classification. In addition, the good prediction results can be achieved with only a short segment of time-domain data. In all the tests, the length of time-domain data is 1024 points, or about 0.1s. In comparison, traditional spectrum analysis methods with MCSA often require several seconds or longer data in order to stably identify the fault components, on top of the domain knowledge required to identify the fault signatures. These advantages make the proposed TDA method promising to be applied to a broad range of fault detection tasks.

VI. Conclusions

In this paper, we apply the topological data analysis to the motor eccentricity fault. The procedure of extracting topological features of time-domain phase current data and converting them into vectorized Betti sequence is introduced and is applied to the analysis of data from different eccentricity levels. We show that this model-free method is very effective in differentiating data that look similar in the time domain, and is applicable to the data-driven motor fault detection and quantification with both interpolation and extrapolation capabilities.

VII. Acknoledgement

The authors thank AKM Khaled Ahsan Talukder for helpful discussions.

References

[1] W. T. Thomson and I. Culbert, *Current signature analysis for condition monitoring of cage induction motors: Industrial application and case histories*. John Wiley & Sons, 2017.

[2] M. E. H. Benbouzid, "A review of induction motors signature analysis as a medium for faults detection," *IEEE transactions on industrial electronics*, vol. 47, no. 5, pp. 984–993, 2000.

[3] S. Nandi, H. A. Toliyat, and X. Li, "Condition monitoring and fault diagnosis of electrical motors—a review," *IEEE transactions on energy conversion*, vol. 20, no. 4, pp. 719–729, 2005.

[4] X. Li, Q. Wu, and S. Nandi, "Performance analysis of a three-phase induction machine with inclined static eccentricity," *IEEE Transactions on Industry Applications*, vol. 43, no. 2, pp. 531–541, 2007.

[5] J. Faiz and B. M. Ebrahimi, "Static eccentricity fault diagnosis in an accelerating no-load three-phase saturated squirrel-cage induction motor," *Progress in electromagnetics research*, vol. 10, pp. 35–54, 2008.

[6] M. Akar, "Detection of a static eccentricity fault in a closed loop driven induction motor by using the angular domain order tracking analysis method," *Mechanical Systems and Signal Processing*, vol. 34, no. 1-2, pp. 173–182, 2013.

[7] S. Zhang, S. Zhang, B. Wang, and T. G. Habetler, "Deep learning algorithms for bearing fault diagnostics—a comprehensive review," *IEEE Access*, vol. 8, pp. 29 857–29 881, 2020.

[8] H. A. Toliyat, M. S. Arefeen, and A. G. Parlos, "A method for dynamic simulation of air-gap eccentricity in induction machines," *IEEE transactions on industry applications*, vol. 32, no. 4, pp. 910–918, 1996.

[9] S. Nandi, S. Ahmed, and H. A. Toliyat, "Detection of rotor slot and other eccentricity related harmonics in a three phase induction motor with different rotor cages," *IEEE Transactions on Energy Conversion*, vol. 16, no. 3, pp. 253–260, 2001.

[10] J. Faiz, B. M. Ebrahimi, B. Akin, and H. A. Toliyat, "Comprehensive eccentricity fault diagnosis in induction motors using finite element method," *IEEE Transactions on Magnetics*, vol. 45, no. 3, pp. 1764–1767, 2009.

[11] L. Zhou, B. Wang, C. Lin, H. Inoue, and M. Miyoshi, "Static eccentricity fault detection for psh-type induction motors considering high-order air gap permeance harmonics," in *2021 IEEE International Electric Machines & Drives Conference (IEMDC)*. IEEE, 2021, pp. 1–7.

[12] C. Gunnar, "Topology and data," *Bulletin of the American Mathematical Society*, vol. 46, no. 2, pp. 255–308, 2009.

[13] H. Edelsbrunner, D. Letscher, and A. Zomorodian, "Topological persistence and simplification," in *Proceedings 41st annual symposium on foundations of computer science*. IEEE, 2000, pp. 454–463.

[14] A. Zomorodian and G. Carlsson, "Computing persistent homology," *Discrete & Computational Geometry*, vol. 33, no. 2, pp. 249–274, 2005.

[15] T. Qaiser, Y.-W. Tsang, D. Taniyama, N. Sakamoto, K. Nakane, D. Epstein, and N. Rajpoot, "Fast and accurate tumor segmentation of histology images using persistent homology and deep convolutional features," *Medical image analysis*, vol. 55, pp. 1–14, 2019.

[16] F. A. Khasawneh and E. Munch, "Chatter detection in turning using persistent homology," *Mechanical Systems and Signal Processing*, vol. 70, pp. 527–541, 2016.

[17] V. De Silva and R. Ghrist, "Coverage in sensor networks via persistent homology," *Algebraic & Geometric Topology*, vol. 7, no. 1, pp. 339–358, 2007.

[18] Y. Lee, S. D. Barthel, P. Dłotko, S. M. Moosavi, K. Hess, and B. Smit, "Quantifying similarity of pore-geometry in nanoporous materials," *Nature communications*, vol. 8, no. 1, pp. 1–8, 2017.

[19] Y. Hiraoka, T. Nakamura, A. Hirata, E. G. Escolar, K. Matsue, and Y. Nishiura, "Hierarchical structures of amorphous solids characterized by persistent homology," *Proceedings of the National Academy of Sciences*, vol. 113, no. 26, pp. 7035–7040, 2016. [Online]. Available: https://www.pnas.org/content/113/26/7035

[20] C. Tralie, N. Saul, and R. Bar-On, "Ripser.py: A lean persistent homology library for python," *The Journal of Open Source Software*, vol. 3, no. 29, p. 925, Sep 2018. [Online]. Available: https://doi.org/10.21105/joss.00925

[21] F. Chazal and B. Michel, "An introduction to topological data analysis: fundamental and practical aspects for data scientists," *arXiv preprint arXiv:1710.04019*, 2017.

[22] Y. Umeda, J. Kaneko, and H. Kikuchi, "Topological data analysis and its application to time-series data analysis," *Fujitsu Scientific & Technical Journal*, vol. 55, no. 2, pp. 65–71, 2019.